Journal of Alloys and Compounds 918 (2022) 165617

Contents lists available at ScienceDirect

Journal of Alloys and Compounds

journal homepage: www.elsevier.com/locate/jalcom

Improved mechanical properties of porous nitinol by aluminum alloying

Alexander N. Monogenov[a], Ekaterina S. Marchenko[a], Gulsharat A. Baigonakova[a], Yuri F. Yasenchuk[a], Alexander S. Garin[a], Alex A. Volinsky[a,b,*]

[a] Laboratory of Superelastic Biointerfaces, National Research Tomsk State University, 36 Lenin Ave., Tomsk 634050, Russia
[b] Department of Mechanical Engineering, University of South Florida, 4202 E. Fowler Ave. ENG030, Tampa 33620, USA

ARTICLE INFO

Article history:
Received 22 March 2022
Received in revised form 6 May 2022
Accepted 24 May 2022
Available online 2 June 2022

Keywords:
Porous alloys
Nitinol
Al doping
Mechanical properties
Porous structure
Microstructure

ABSTRACT

Aluminum alloying effects (up to 2 at %) on the macrostructure, microstructure, and mechanical properties of porous nitinol (NiTi) obtained by self-propagating high-temperature synthesis (SHS) were studied. It has been established that Ni and Ti interactions with liquid Al (0.5–1 at % Al) in the SHS process significantly change macrostructure, decrease the size of the interpore bridges, and increase their number, resulting in a larger effective cross-sectional area. An increase in the aluminum content above 1 at % leads to larger interpore bridges in the SHS product. The microhardness of TiNi(Al) increases from 305 $HV_{50\ g}$ to 422 $HV_{50\ g}$ with aluminum concentration, while the fraction of the TiNi(Al) (B2 + B19′) phases decreases from 75% to 50%. The Ti_2Ni(Al) phase fraction increases from 25% to 50% with Al concentration. The 64 MPa tensile strength and 2.9% fracture strain of porous $Ti_{50}Ni_{49}Al_1$ alloy are higher than without Al. The increase in strength is due to the formation of a more homogeneous macrostructure and solid solution strengthening of the alloy-forming phases.

1. Introduction

Bulk and porous nitinol (NiTi) alloys are a promising class of metal implants due to their high corrosion resistance and deformation behavior similar to the bone tissues of the human body [1,2]. A convenient tool for controlling corrosion and mechanical properties is aluminum alloying of nitinol [3–6]. Studies of nitinol alloyed with aluminum were carried out by others using alloys obtained by casting, additive technologies, and powder metallurgy [7–9]. In addition to a variety of nickel and titanium aluminides, calculated and experimental phase diagrams of the NiTiAl system show the presence of multiple ternary compounds: $Al_{13}Ni_2Ti_5$, Al_2NiTi, Al_3NiTi_2, and $AlNi_2Ti$ [10–14]. Monolithic NiTi alloyed with 6–9 at % Al has increased ultimate compressive strength, and the martensitic shear stress [6]. The reason for the favorable aluminum alloying effects on the bulk nitinol strength lies in the solid solution hardening of the B2 phase with aluminum atoms. Depending on the composition and temperature, numerous chemical reactions between the components have been studied. The sintering mechanisms of the TiNiAl system have been studied by X-ray diffraction, elemental analysis, differential thermal analysis, and electron microscopy [15]. The obtained NiTi alloy consisted of the TiNi, Ti_2Ni, and $AlNi_2Ti$ phases.

Implants based on porous NiTi must withstand significant loads without fracture because they are mainly used to replace bones. Thus, the problem of obtaining high-strength porous NiTi alloys is quite relevant. Porous NiTi alloys obtained by powder metallurgy are characterized by structural anisotropy and chemical inhomogeneity [16–22]. Due to this problem, physical and mechanical properties vary greatly and depend both on the properties of the initial powders (chemical purity, granulometric composition and specific surface area of particles, manufacturing method) and additional thermomechanical treatment [23]. The macroscopic properties of intermetallic compounds obtained by the SHS method are primarily affected by the dissolution of components with subsequent crystallization of compounds from the melt or the formation of compounds upon their direct contact due to diffusion reactions [24]. A particularly intense interaction in metallic systems is observed when a liquid phase appears, which is formed either due to the melting of low-melting temperature components or during the eutectic formation [24]. NiTi alloying with aluminum is of particular interest for manufacturing alloys by self-propagating high-temperature synthesis (SHS). It is assumed that aluminum enhances the interaction of titanium and nickel at the diffusion reaction stage, significantly changing the SHS process kinetics, and, as a consequence, the structural phase anisotropy of the final product. The literature

* Corresponding author at: Department of Mechanical Engineering, University of South Florida, 4202 E. Fowler Ave. ENG030, Tampa 33620, USA
E-mail address: volinsky@usf.edu (A.A. Volinsky).

https://doi.org/10.1016/j.jallcom.2022.165617
0925-8388/

contains limited information regarding aluminum alloying effects on the structure and properties of SHS NiTi alloys [25–28].

In this study, the concentration range of Al is determined by using the size and electronic Hume-Rothery factors. In reference [29] it has been assumed that aluminum atoms can occupy both the titanium and nickel sublattices. The purpose of the work is to improve the physical and mechanical properties of porous NiTi alloys by aluminum alloying and forming a homogeneous macrostructure.

2. Materials and methods

Porous NiTi alloys with different aluminum concentrations of 0.5 at %, 1 at %, 1.5 at %, and 2 at % were obtained by the SHS method under the same thermodynamic conditions according to the procedures described in [30,31]. Powders of titanium, nickel, and aluminum were preliminarily dried in an electric vacuum oven at 70–80 °C for 7 h. To prepare the samples, nickel, titanium, and aluminum powders were sieved to obtain uniform particle sizes. The average size of titanium, nickel, and aluminum powders was 16 μm, 5 μm, and 9 μm, respectively. The obtained samples were 300 mm long with 12 mm diameter. The porosity of 62–66% was determined by weighing [32]. When calculating the initial charge composition, some of the nickel atoms were replaced by aluminum atoms.

Macro and microstructure analysis was performed using a Tescan Vega-3 SBH scanning electron microscope equipped with an Oxford Instruments AztecLive Lite Xplore 30 energy dispersive spectroscopy (EDS) system. The survey was carried out at an accelerating voltage of 20 kV.

The phase composition was investigated by X-ray diffraction analysis (XRD) using the Shimatsu XRD-6000 diffractometer with Cu Kα radiation (1.541 Å wavelength) at 40 kV and 30 mA. Surveys were carried out at 10–80° 2θ diffraction angle range with a 0.02° step and 1°/min scan speed. To identify the XRD spectra, the POWDER CELL 2.4 full-profile analysis program and PDF4 + crystal structure database were used.

The tensile strength was measured using plate specimens 2.5 mm × 2.5 mm× 30 mm in size, cut from porous ingots by the electrical discharge machining (EDM). Using the ImageJ (Wayne Rasband, NIH) software, the average effective cross-sectional area of the samples was obtained, and the tensile strength of porous NiTi samples doped with aluminum was determined by dividing the load by the measured area [33]. The Vickers microhardness of the phases was measured using the Metolab-502 microhardness tester at a 50 g load. The number of measurements was 15 per phase.

2.1. Aluminum alloying limits of porous NiTi alloys

The Hume-Rothery rules were used to obtain the maximum concentration of the alloying element at which the B2 and B19′ phases formation was possible [34]. The Hume-Rothery size factor for the binary system is calculated as:

$$\delta = \left|1 - \frac{R_A}{R_B}\right| \quad (1)$$

Here, R_A is the atomic radius of the element being dissolved and R_B is the atomic radius of the matrix element. Using these calculations, one can choose the limiting concentration of the aluminum alloying element and predict which sublattice will be occupied by aluminum atoms in the case of the solid solution formation of Al in the NiTi alloy without the formation of ternary phases. The calculation of the valence electrons concentration, e/atom, which is determined by the number of electrons in the unfilled outer shell per atom, was carried out for a three-component system, as in [34]:

$$e/atom = C_{Ti}Z_{Ti} + C_{Ni}Z_{Ni} + C_{Al}Z_{Al} \quad (2)$$

$$C_{Ti} + C_{Ni} + C_{Al} = 1 \quad (3)$$

Here, C_{Ti}, C_{Ni}, and C_{Al} are the concentrations of the corresponding elements in relative units, and Z_{Ti}, Z_{Ni}, and Z_{Al} are the numbers of electrons in the outer shells of Ti, Ni, and Al, respectively.

For porous alloys to have high physical and mechanical properties, while exhibiting shape memory and superelasticity effects, it is necessary to take into account the physicochemical properties of the alloy-forming elements when choosing the Al concentration range. Hume-Rothery established dimensional and electronic factors influencing the dissolution of alloying components in the B2 phase. Extending these ideas to nickel-titanium alloys doped with a third element, one can estimate its maximum concentration, which dissolves in the B2 phase, and is capable to participate in martensitic transformations. In some cases, it is possible to determine whether Ti or Ni will be replaced when the alloying element is dissolved. According to the triple-phase diagram, there is only a small 47–51 at % Ni region of homogeneity of the NiTi phase in the Al-Ti-Ni ternary system, which has a round shape without predominantly spreading towards any element. However, this method does not predict which element will be replaced by aluminum [10]. Corresponding parameters for titanium, nickel, and aluminum, listed in the periodic table of the elements, were used in calculations [35].

Let's consider a three-component system formed as a result of alloying a NiTi alloy with aluminum. According to [34], the implementation of the following four dissolution options is possible:1. Aluminum atoms replace only titanium atoms, in which case the "effective" atom (Ti, Al) has the radius:

$$R_{Ti,Al} = C_{Ti}^{Ti}R_{Ti} + C_{Al}^{Ti}R_{Al} \quad (4)$$

Here, C_{Ti}^{Ti} and C_{Al}^{Ti} are the concentrations of Ti or Al atoms in the Ti sublattice, which are dissolved in the nickel-based crystalline matrix. The corresponding size factor is:

$$\delta_1 = \left|1 - \frac{R_{Ti,Al}}{R_{Ni}}\right| \quad (5)$$

2. Aluminum atoms replace only nickel atoms, and the "effective" atom (Ni, Al) has the radius:

$$R_{Ni,Al} = C_{Ni}^{Ni}R_{Ni} + C_{Al}^{Ni}R_{Al} \quad (6)$$

Here, C_{Ni}^{Ni} and C_{Al}^{Ni} are the concentrations of Ni or Al atoms in the Ni sublattice, which dissolve in the titanium-based crystalline matrix. The corresponding size factor is:

$$\delta_2 = \left|1 - \frac{R_{Ni,Al}}{R_{Ti}}\right| \quad (7)$$

3. The alloying element is titanium, which dissolves in a crystalline lattice composed of "weighted average" atoms (Ni, Al) with a radius calculated using Eq. (6). In this case, the expression for the size factor is:

$$\delta_3 = \left|1 - \frac{R_{Ti}}{R_{Ni,Al}}\right| \quad (8)$$

4. The alloying element is nickel, which dissolves in a crystalline lattice composed of "weighted average" atoms (Ti, Al) with a radius calculated using Eq. (4). The size factor in this case is:

$$\delta_4 = \left|1 - \frac{R_{Ni}}{R_{Ti,Al}}\right| \quad (9)$$

Fig. 1 plots the Hume-Rothery size factor δ as a function of Al concentration for all considered cases. It is known that more than half of the phases with a B2 superstructure (out of more than 900) exist at $\delta > 0.15$, and at $\delta > 0.25$ these phases are completely stable to structural phase transformations [35]. These border areas are indicated by the horizontal dashed lines in Fig. 1.

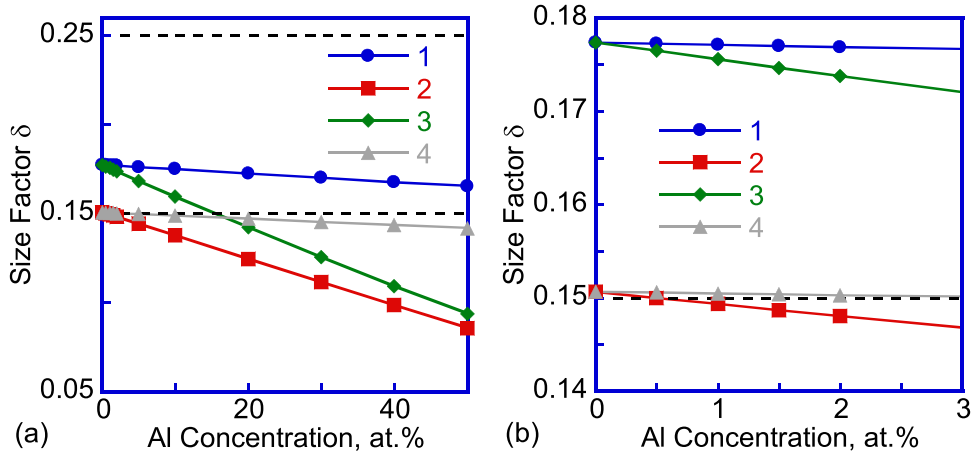

Fig. 1. The Hume-Rothery size factor δ as a function of Al concentration for the four considered cases: (a) 50 at % Al concentration range and (b) 3 at % Al concentration range. Case 1 - aluminum atoms replace only titanium atoms, which dissolve in the nickel-based crystalline matrix. Case 2 - aluminum atoms replace only nickel atoms, which dissolve in the titanium-based crystalline matrix. Case 3 - titanium dissolves in the crystal lattice, composed of "weighted average" (Ni, Al) atoms. Case 4 - the alloying element is nickel, which dissolves in the crystal lattice, composed of "weighted average" atoms (Ti, Al).

Thus, in the first case, atoms with a "weighted average" radius $R_{Ti,Al}$, calculated using Eq. (4), in the 1.445–1.46 Å range, replace nickel atoms R_{Ni}, which have a 1.24 Å size. On the contrary, in the fourth case, nickel atoms replace "weighted average" atoms in the lattice with $R_{Ti,Al}$. The authors assumed that of these two, the 4th case is most likely to be realized since replacing atoms of a smaller radius with atoms of a larger one requires more energy than embedding atoms with a smaller radius into a crystal lattice with atoms of a larger radius (Fig. 1, case 4).

Next, consider cases 2 and 3. In the 2nd case, atoms with a "weighted average" radius $R_{Ni,Al}$ calculated using Eq. (6) in the 1.24–1.335 Å range replace titanium atoms R_{Ti}, which have a 1.46 Å size. The 3rd case describes the dissolution of titanium atoms with a larger radius in a lattice built of atoms with a smaller "weighted average" radius $R_{Ni,Al}$.

It can be assumed that the 2nd case is the most probable (Fig. 1, case 2). Thus, there are two most likely options left for consideration - cases 2 and 4. In the 2nd case when aluminum atoms replace only nickel atoms, increasing the "weighted average" radius $R_{Ni,Al}$, and dissolve in the titanium lattice at all Al concentrations, the B2 phase is not formed. This suggests that such an option is not possible, since numerous studies of the TiNiAl system prove that there is a B2 phase in this system. Therefore, there is only one conclusion that the Hume-Rothery size factor shows the formation of the B2 phase only in a limited Al concentration range. Al concentration should not exceed 2 at %. In this case, aluminum replaces titanium atoms. The size factor dependence on the aluminum concentration shows that along with the B2 phase, secondary phases will precipitate since aluminum does not form an unlimited solid solution in the B2 phase.

Another important parameter that affects the phase stability is the electron density of valence electrons *e*/atom, which is determined by the number of electrons in the unfilled outer shells per atom [34,36]. The electron density of the NiTi system was calculated using Eqs. (2) and (3). The B2 phase homogeneity region is between 6.88 *e*/atom and 7.36 *e*/atom, represented by the dashed lines in Fig. 2. As seen in Fig. 2(a), the substitution of titanium atoms with aluminum atoms imposes a limitation on the Al concentration of 12 at % (Fig. 2(a), blue, $Ti_{50-x}Ni_{50}Al_x$). If aluminum atoms occupy sites on the nickel sublattice (replacing Ni atoms), a decrease in the electron density is observed with increasing Al concentration (Fig. 2(b), red, $Ti_{50}Ni_{50-x}Al_x$). In this case, the maximum content of the alloying element at which it can dissolve in the $Ti_{50}Ni_{50-x}$ matrix while maintaining the B2 structure is approximately 2 at %.

Analysis of the dimensional and electronic Hume-Rothery factors for the TiNiAl system showed that aluminum atoms can occupy both titanium and nickel positions. It is assumed that aluminum will

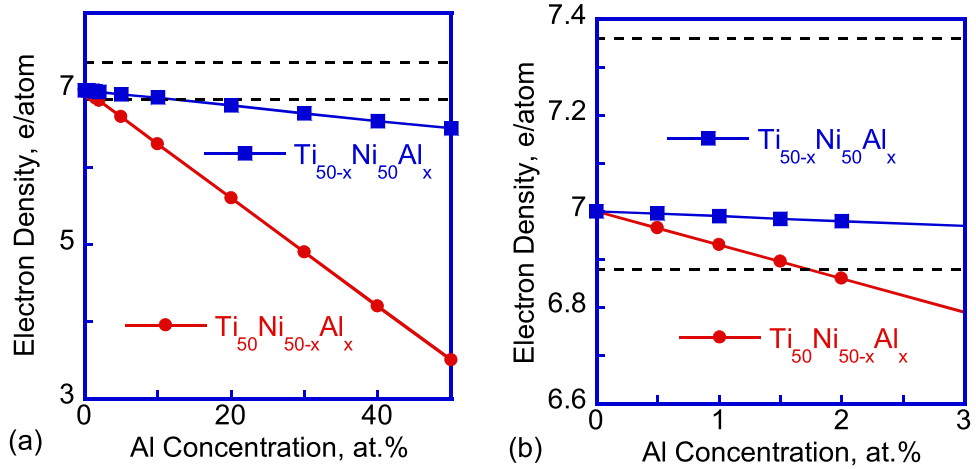

Fig. 2. Electron density (the number of free electrons per atom) as a function of Al concentration for the $Ti_{50-x}Ni_{50}Al_x$ and $Ti_{50}Ni_{50-x}Al_x$ systems: (a) 50 at % Al concentration range and (b) 3 at % Al concentration range.

occupy all vacancies on the titanium sublattice first since the solubility of aluminum in the titanium sublattice is 6 times higher than in the nickel sublattice. Only then will the aluminum settle in the positions of the nickel atoms. Excess aluminum will dissolve in secondary phases, presumably Ti_2Ni. Therefore, to minimize the number of secondary phases, it seems most promising to choose 0.5–2 at % Al concentration range for alloying porous NiTi alloys. Even a slight decrease in the number of titanium atoms causes NiTi alloys embrittlement, while the martensitic plateau disappears in stress-strain curves [18]. The material is no longer able to withstand cyclic loading, becomes brittle, and fractures.

2.2. Macrostructure of porous TiNiAl alloys

The effects of aluminum alloying on the porous framework macrostructure were studied by comparing the effective cross-sectional area of all samples, the specific surface area of the framework, and the size distribution of monolithic bridges of the porous framework. In order to quantitatively show the effects of aluminum alloying, the cross-sectional SEM images were processed to enhance the contrast and converted into a binary form. Size distribution histograms of the bulk interpore bridges were obtained (Table 1). It was found that the porous macrostructure of the SHS NiTi alloy has

Table 1
Macrostructure and size distribution of interpore bridges in the cross-section of porous SHS NiTi alloys.

Alloy	Sample cross-section	Bridges size distribution
No Al	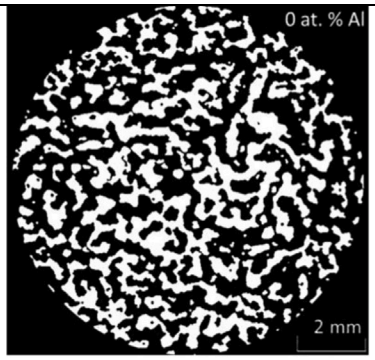	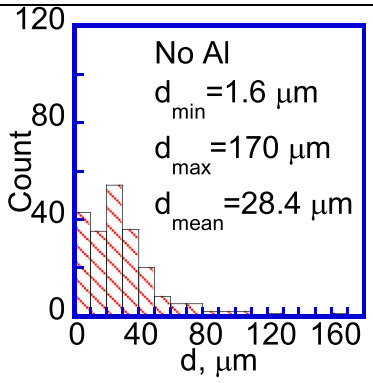
0.5 at.% Al	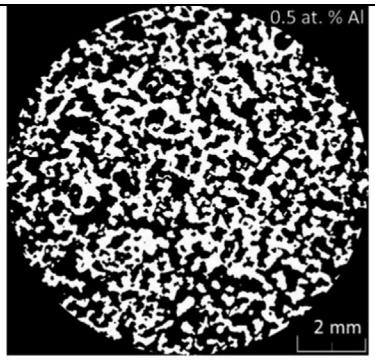	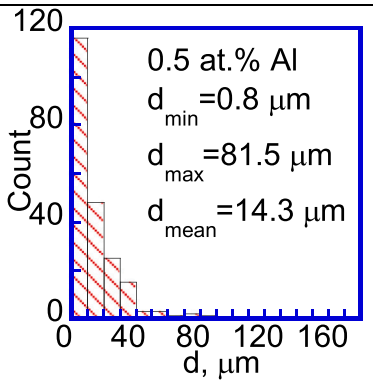
1 at.% Al	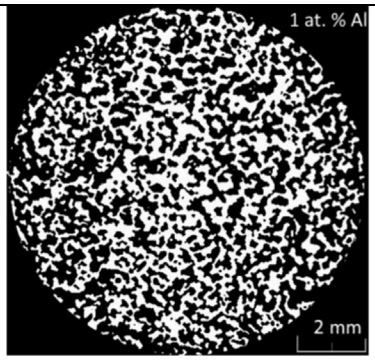	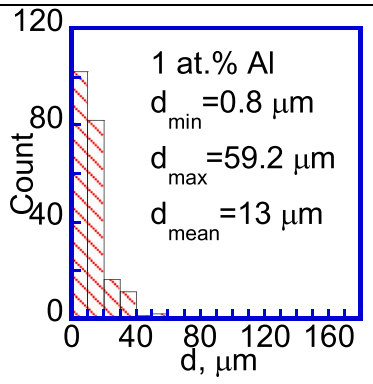

(continued on next page)

Table 1 (*continued*)

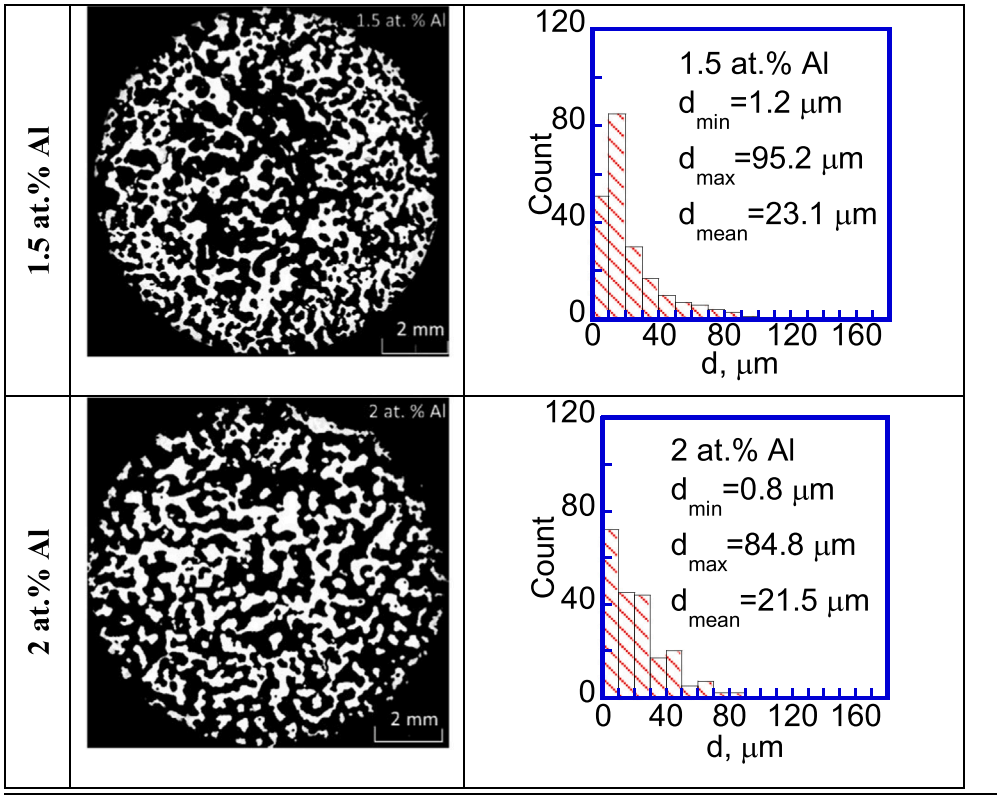

already undergone noticeable changes with a minimum of 0.5 at % Al alloying. With the addition of 1 at % Al, a more uniform and dispersed system of pores with a large number of bridges was formed. The size distribution of the bridges showed that the number of thick bridges was significantly reduced. The average bridge size was reduced from 28 μm without Al to 13 μm with Al alloying, but the number of 1–20 μm bridges was increased. The maximum bridge size was reduced from 170 μm for an unalloyed porous SHS NiTi to 60 μm, which corresponds to the most homogeneous $Ti_{50}Ni_{49}Al_1$ alloy.

The effective cross-sectional area of the porous framework increases from 31.5 mm^2 to 34 mm^2 when alloyed with up to 1 at % aluminum, and then sharply decreases to 29.5 mm^2 with higher Al concentration in Fig. 3. The specific porous framework surface area dependence on the Al concentration also shows a sharp maximum at 1 at % Al in Fig. 4. The formation of a more homogeneous macrostructure of the porous framework with a noticeable increase in the specific surface increases the strength by reducing the internal stresses of monolithic bridges during the loading of the samples.

2.3. Microstructure and elemental composition of porous NiTiAl alloys

Porous SHS NiTi compounds doped with aluminum are represented by a two-phase system consisting of primary dendritic and interdendritic phases (Table 2). X-ray spectral microanalysis, conducted at 10 similar areas on one sample, showed that the initial dendritic phase is $Ti_2Ni(Al)$. The composition of the interdendritic

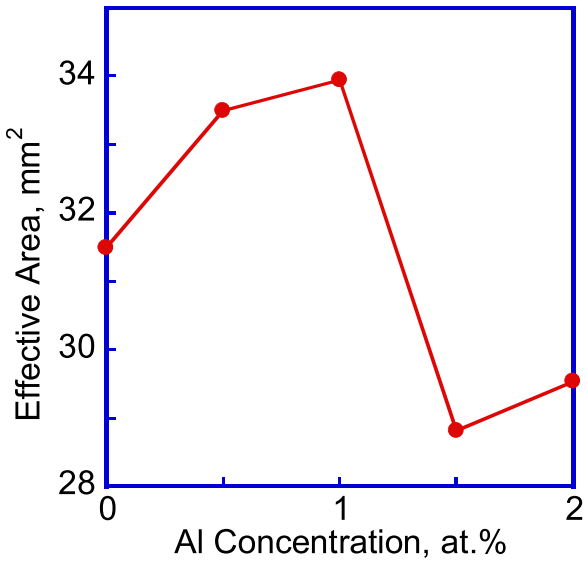

Fig. 3. The effective cross-sectional area of the porous framework as a function of Al concentration.

phase was determined as TiNi(Al). With higher aluminum content, aluminum concentration increases in both TiNi(Al) and $Ti_2Ni(Al)$ phases of the final SHS product in Table 3.

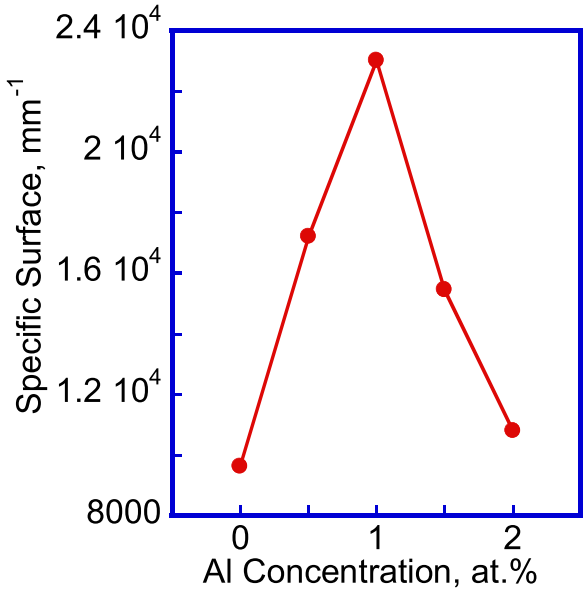

Fig. 4. The specific surface of the bridges of the porous framework as a function of Al concentration.

Elemental mapping shows that aluminum is contained mostly in the Ti_2Ni phase (Table 2). The exception is a compound with 1 at % aluminum. When the concentration ratio $C_{Al}(Ti_2Ni)/C_{Al}(TiNi)$ is less than 2, which corresponds to the porous $Ti_{50}Ni_{49}Al_1$ alloy, it is difficult to determine which phase contains more aluminum from the aluminum distribution maps (Table 2).

X-ray spectral microanalysis, carried out in 10 areas in the peritectic zones of each of the samples, showed an approximate correspondence of the measured concentration composition to the stoichiometric composition of the Ti_2Ni and TiNi compounds. The ratio of titanium to nickel practically does not change with higher Al concentration, neither in the TiNi, nor in the Ti_2Ni phases in Fig. 5. Therefore, it can be assumed that the temperature ranges of direct and reverse martensitic transformations in porous TiNiAl alloys should not undergo significant changes. The concentration of aluminum in the Ti_2Ni phase is approximately 2 times higher than in the TiNi phase. This can be explained by the low solubility of aluminum in the TiNi phase, and because the Ti_2Ni phase and liquid aluminum solidify later than the TiNi phase.

Let's consider in more detail the features of the zone of peritectic crystallization (Ti_2Ni+TiNi) of porous SHS NiTi doped with aluminum. Using scanning electron microscopy, it was established that the grains of the TiNi phase are surrounded by the intergranular Ti_2Ni phase, in which dispersed aluminum inclusions are concentrated during peritectic crystallization in Fig. 6.

It should be noted that the impurity phase only exists in an isotropic dispersed form at 1 at % Al in Fig. 6(b), but at other concentrations Al forms dendrites. An increase in the anisotropy of the inclusions' distribution in the intergranular region with more Al observed in Al distribution maps, is expressed in the formation of dendrites with Al impurities. Violation of the monotonic growth of structural anisotropy at 1 at % Al did not find an explanation. Inclusions containing a large amount of Al appear in the interdendritic zone with a minimal 0.5 at % Al addition. In this case, the surface of the TiNi phase grains becomes noticeably rougher, indicating that coalescence and smoothing of primary grains by dispersed Al inclusions slowed down. At 1 at % Al, the density of inclusions decreases abnormally, and at 1.5 at % it continues to increase. At 1–1.5 at % Al concentration the grains become large again with a smoother surface, and at 2 at % Al, the process of coalescence of primary grains is inhibited. The density of inclusions in the interdendritic phase at 2 at % Al is the maximum.

2.4. Phase composition of porous TiNiAl alloys

X-ray diffraction analysis in Fig. 7 demonstrates that porous Al-doped NiTi alloys consist only of TiNi and Ti_2Ni binary compounds the same way as before alloying. No ternary phases with aluminum were found, however, it was found that the unit cell parameters of the TiNi and Ti_2Ni phases increased with Al concentration in Fig. 8. In this case, a more intense increase in the lattice parameter of the Ti_2Ni phase was observed, which correlates with the elemental analysis data. Aluminum atoms are intermediate in size between titanium and nickel atoms. Therefore, it can be assumed that aluminum atoms (according to the substitution scheme) occupy the positions of nickel atoms, since if they occupied the positions of titanium atoms, then the unit cell parameter would have to decrease. The second option for aluminum alloying atoms would be to occupy interstitial sites.

A certain fraction of the martensitic phase TiNi (B19′) was found in all samples (Table 4). Before alloying, it was 32 vol % and decreased to 9 vol % with alloying, which indirectly indicates a decrease in internal stresses in the alloy as a result of the Al addition. It has been established that aluminum atoms form solid solutions with TiNi and Ti_2Ni intermetallic compounds, occupying the positions of nickel atoms or interstices and creating additional internal stresses in the crystal lattice. This leads to an increase in the microhardness of the TiNiAl alloys.

When alloyed with aluminum, the proportion of the high-temperature TiNi (B2) phase was more than 40 vol %, the same as without Al. However, at 1 at % and 2 at % Al, the proportion of the B2 phase decreases to 30 vol % and 33 vol %, respectively. The porous NiTi alloy without aluminum is characterized by the fact that the proportions of Ti_2Ni and TiNi (B2 +B19′) are maximally different. With Al alloying, their fractions begin to converge and equalize at 2 at % Al in Fig. 9.

The symmetrical change in the proportions of Ti_2Ni and TiNi is a consequence of titanium segregation during the peritectic crystallization of austenite. It can be argued that an increase in the aluminum concentration enhances the segregation process, bringing it to the limit at 2 at % Al, when the proportions of Ti_2Ni and TiNi are equalized.

Before the crystallization of the Ti_2Ni phase, a peritectic melt existed around the TiNi grains, the proportion of which increased due to an increase in the segregation intensity during the peritectic crystallization of the TiNi phase. There is an obvious direct correlation between an increase in the amount of a low-melting aluminum alloying additive, with an increase in the proportion of the peritectic melt during the synthesis of the porous alloy, and the proportion of the Ti_2Ni phase after the alloy crystallization.

Table 2
Microstructure and distribution maps of Al, Ti, and Ni in porous TiNiAl alloys. (1 - TiNi, 2 - Ti_2Ni).

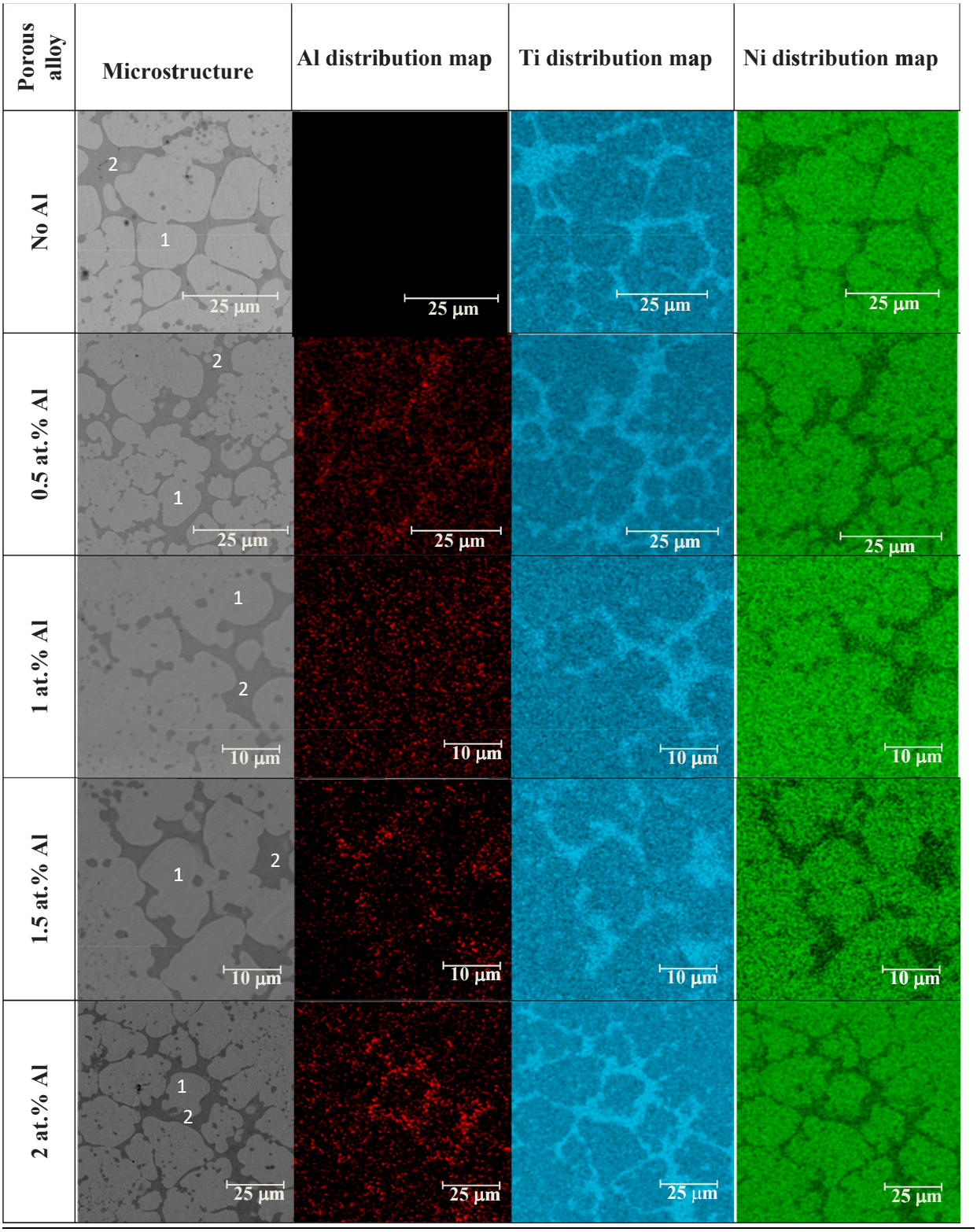

2.5. Microhardness and mechanical properties of TiNiAl alloys

The Vickers microhardness of porous TiNiAl alloys was measured in the peritectic region at a 50 g load. With an increase of aluminum concentration from 0 to 2 at %, the microhardness of porous NiTi alloys increases from 305 HV to 422 HV with a decrease in the proportion of the TiNi (B2 +B19′) phase from 75% to 50% and an increase in the proportion of the Ti_2Ni phase from 25% to 50% in Table 5. The established average microhardness value for the porous TiNi alloy without aluminum correlates with the literature data

Table 3
X-ray spectral microanalysis data in %.

Porous alloy	TiNi(Al)			Ti_2Ni(Al)		
	Al	Ti	Ni	Al	Ti	Ni
No Al	0.15	51.16	48.69	0.04	64.23	35.73
0.5 at % Al	0.62	50.94	48.44	1.74	65.3	32.96
1 at % Al	0.57	50.98	48.45	0.97	66.73	32.3
1.5 at % Al	0.78	50.98	48.24	1.94	65.51	32.55
2 at % Al	0.8	50.75	48.45	2.06	65.69	32.25

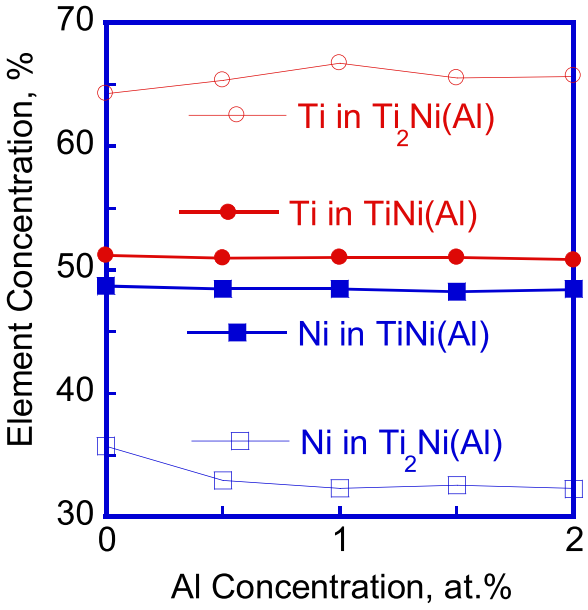

Fig. 5. Ti and Ni concentrations in the TiNi and Ti_2Ni phases obtained from the X-ray diffraction microanalysis.

[37–41]. Thus, it was established that alloying with aluminum led not only to a change in the macrostructure of the porous framework but also to an increase in the microhardness of monolithic bridges, probably due to an increase in the volume of the Ti_2Ni(Al) phase.

Deformation of porous samples with 0.5–2 at% Al was studied by the uniaxial tensile tests together with a control sample synthesized without aluminum. Stress-strain curves of uniaxial tension (Fig. 10), cumulative elongation to failure, martensitic shear stress, and ultimate strength were obtained, which were converted into stresses using the calculated results of the effective cross-sectional area.

It has been established based on the uniaxial tension to failure tests that the NiTi alloy with 1 at % Al has a tensile strength, maximum strain to failure, and martensitic shear stress 1.8–2 times higher than without Al (Fig. 10, Table 6). All stress-strain curves have yield regions caused by the transformation of austenite into martensite, which began at the critical martensitic shear stress σ_m. The areas of elastic deformation and the yield plateau coincide for all samples, except for the 1 at % Al. The tensile strength of the 0.5–1 at % Al samples monotonically increases from 37 MPa to 64 MPa with aluminum concentration, but at 2 at % Al sharply drops to 44 MPa. A comparison of the stress-strain curves showed that an increase in the Al concentration past 0.5 at % leads to a non-linear change in martensitic shear stress, tensile strength, and accumulated strain (Table 6).

The strength and deformation characteristics are inversely related to the thickness of the bridges of the porous framework (see Table 1). Porous alloy with 1 at % Al has the highest strength since an increase in the number of bridges and their uniform thickness leads to an increase in the effective cross-sectional area, which in turn leads to a decrease in the average load per bridge. The martensitic shear stress of the porous alloy with 1 at % Al, which has the largest effective cross-sectional area, turned out to be almost 5 MPa higher than the analogous parameter of all other samples. This can be explained by the lower level of internal stresses in $Ti_{50}Ni_{49}Al_1$ porous alloys compared with all other alloys. Therefore, it is necessary to apply higher external stress for martensite nucleation than for other compositions of the TiNiAl system. The fracture load attributable to small bridges and the total accumulated deformation in a finely porous sample turned out to be higher compared to all other samples. As a result, the ultimate strength of the finely porous sample turned out to be 20–35 MPa higher than the other samples.

3. Discussion

It is known that during SHS of porous nitinol and layer-by-layer combustion, the evolution of the porous framework has the following sequence [42]:1. The formation of the reaction layer begins with the entry of the first portion of the eutectic liquid into the heated layer and spreads over the porous charge as a result of the action of the capillary forces. As a result of the eutectic liquid spreading, a reaction zone is formed, in which the titanium and nickel reagents partially dissolve in the eutectic liquid and enter into a liquid-phase heterogeneous exothermic reaction for the synthesis of nitinol. A new portion of the eutectic liquid is formed at about 1300 °C, which again spreads under the action of capillary forces over the adjacent volume of the heated porous charge, dissolving it. In this case, the released heat of the reaction is spent on heat and mass transfer, which consists of conductive and convective heat transfer of the eutectic liquid by the reaction gases. Thus, there is a self-propagation of the exothermic reaction of nitinol synthesis.2. The addition of Al, which has a melting point of 610 °C, lowers the appearance of the liquid phase by 300 °C against the background of an insufficiently heated charge [43]. Compared to the temperature of the appearance of eutectics in Ti-Ni interparticle contacts, the temperature range of the peritectic crystallization reaction increases. These factors increase the amount of liquid phase in the reaction zone. An increased amount of melt accelerates the coalescence of small pores into large ones. This leads to an increase in the proportion of large pores and an increase in the anisotropy of the porous framework.3. The crystallization temperature of ternary intermetallic compounds with an admixture of Al, $NiAl_3$, and $TiAl_3$ intermetallic compounds are higher than the TiNi, Ti_2Ni, and $TiNi_3$ intermetallic compounds, which creates additional crystallization centers in the peritectic crystallization front. With more aluminum, the proportion of $NiAl_3$ and $TiAl_3$ refractory phases and the number of crystallization centers increase, which increases the surface tension force and reduces the propagation velocity of the combustion

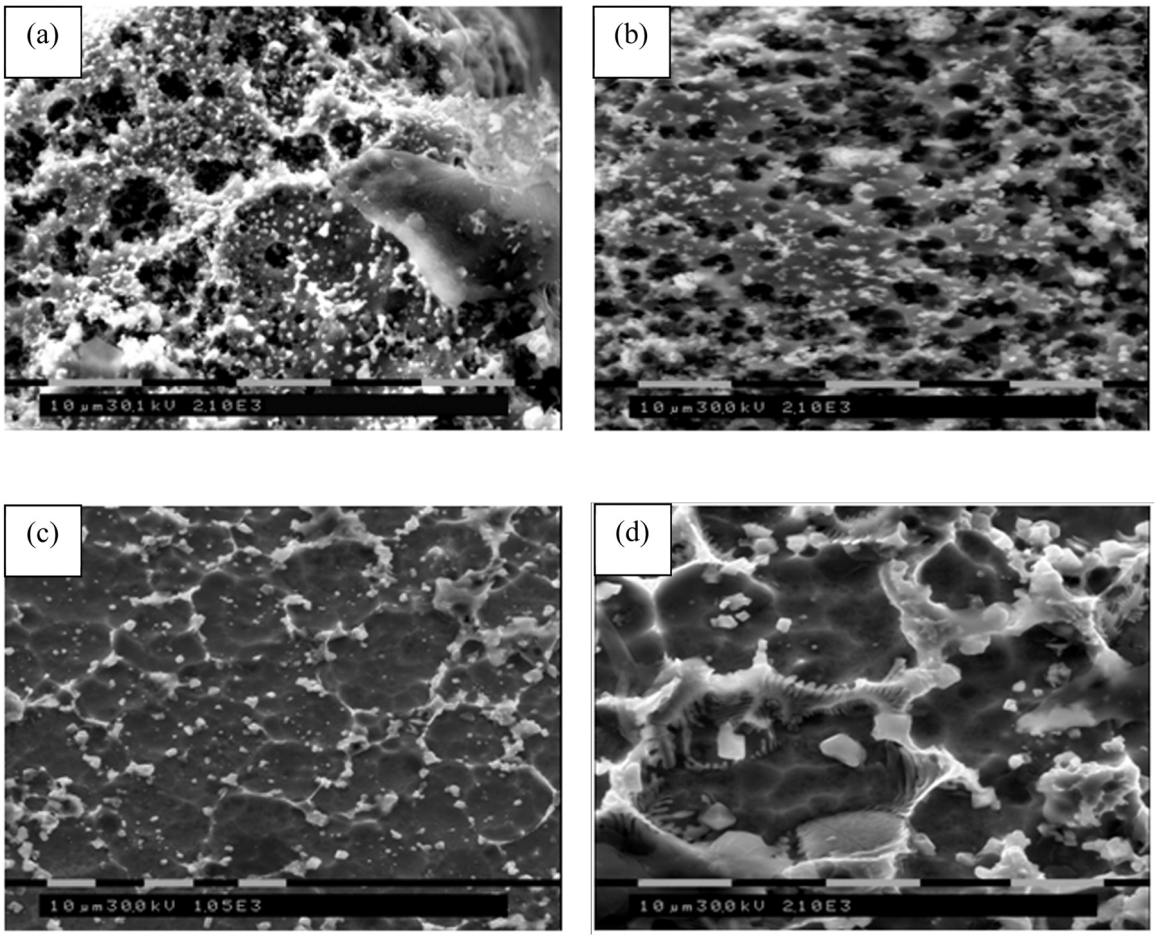

Fig. 6. Crystallization of dendrites in the peritectic zone (Ti_2Ni+TiNi) of porous SHS NiTi alloys with the addition of Al: (a) 0.5 at %, (b) 1 at %, (c) 1.5 at %, and (d) 2 at %.

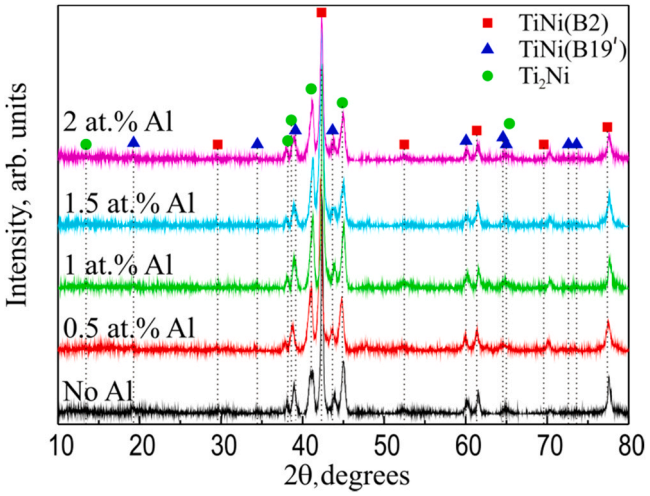

Fig. 7. X-ray diffraction patterns of porous NiTi alloys with 0–2 at % Al.

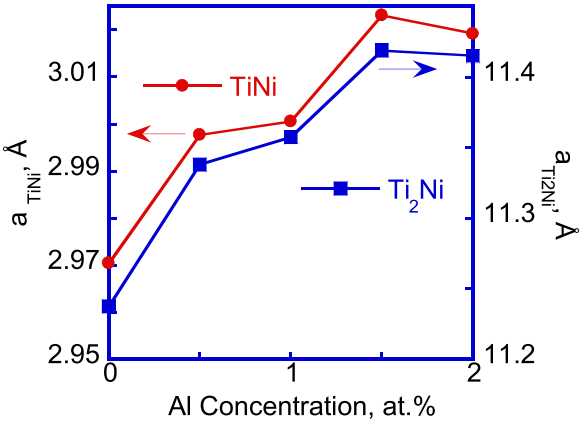

Fig. 8. The lattice parameter of the TiNi(Al) B2 and Ti_2Ni(Al) phases.

wavefront.4. Heat and mass transfer of the eutectic liquid in the finely porous heating zone under the action of capillary forces form a new reaction zone. At the same time, most of the eutectic liquid is transferred by the reaction gases in the opposite direction to the large-pore structure zone, which has a much lower resistance to gases than the fine-pore heating zone. In the structure zone, the liquid carried by the reaction gases condenses on the surface of large pores and forms a large-pore framework. In addition, the heat transferred from the reaction zone heats the surface of the porous framework and stimulates the formation of zones of peritectic crystallization of the porous framework, in which dendrites are

Table 4
The volume fraction of phases and ratio of aluminum concentration in Ti_2Ni and TiNi phases of porous NiTi alloys.

Porous alloy	Ni/Ti ratio in TiNi (B2)	C_{Al} (Ti_2Ni)/C_{Al} (TiNi)	$V_{Ti2Ni\ (Al)}$ %	$V_{TiNi\ (Al)}$ (B2) %	$V_{TiNi\ (Al)}$ (B19′) %	V_{total} %
No Al	0.95	–	25	42	32	99
0.5 at % Al	0.95	2.8	32	45	22	99
1 at % Al	0.95	1.7	45	30	24	99
1.5 at % Al	0.946	2.48	45	46	9	100
2 at % Al	0.956	2.58	50	33	17	100

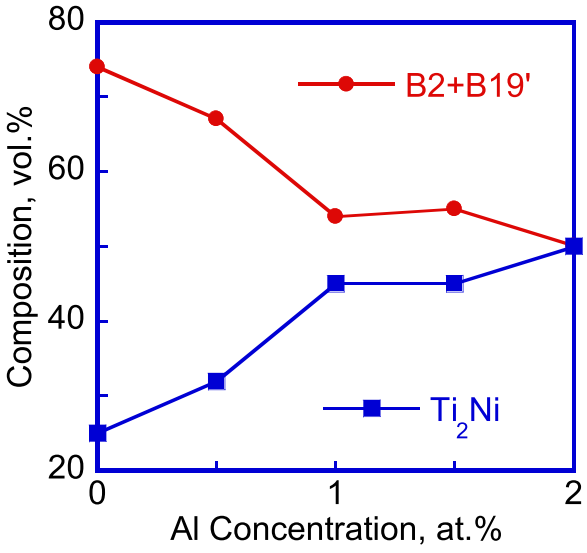

Fig. 9. Composition of TiNi(Al) phases (sum of the B2 and B19′ phases compositions) and Ti_2Ni(Al) in porous NiTi alloyed with aluminum.

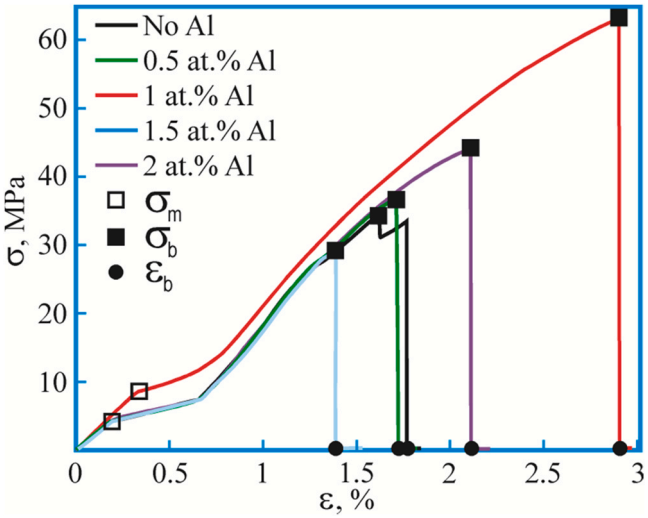

Fig. 10. Stress-strain curves of SHS porous NiTi alloys with varying Al concentration.

Table 5
Vickers microhardness of the TiNi and Ti_2Ni phases in porous SHS NiTi specimens alloyed with aluminum.

Phase microhardness $HV_{50\ g}$	No Al	0.5 at % Al	1 at % Al	1.5 at % Al	2 at % Al
TiNi+ Ti_2Ni	305 ± 28	334 ± 30	344 ± 32	416 ± 39	422 ± 41

Table 6
Strength properties of porous SHS NiTi alloys with various Al concentrations.

NiTi alloy	S_{eff}, mm^2	σ_b, MPa	ε_b, %	σ_m, MPa
No Al	2.57 ± 0.24	34	1.6	4
0.5 at % Al	2.77 ± 0.23	37	1.7	4
1 at % Al	2.88 ± 0.22	64	2.9	8
1.5 at % Al	2.41 ± 0.21	29	1.4	4
2 at % Al	2.45 ± 0.24	44	2.1	4

Here, S_{eff} is the effective cross-sectional area $S_{eff} = S_{All}$-S_{pores}; σ_b is the tensile strength; ε_b is the fracture strain or the appearance of the first crack; σ_m is the martensitic shear stress.

formed from large TiNi grains surrounded by peritectic intergranular melt.5. Dissolved and adsorbed impurities in the mixture during the dissolution of Ti and Ni powders undergo thermal dissociation, get partially gasified, and are transferred by reaction gases to the structure-forming zone. During condensation and selective crystallization, they form a multilayer structure on the surface of the porous framework. It is known that Al impurities contribute to the amorphization of thin intermetallic layers [44].

Based on the obtained results, it can be argued that Al doping has a complex nonlinear effect on the geometry and phase composition of the porous framework. Al doping mechanisms are determined by two factors. Low-melting aluminum reduces the eutectic appearance temperature by approximately 300 °C and increases its amount [43]. This factor increases the thermal effect of the reaction and the amount of melt in the reaction zone leads to the merging of pores and thickening of the porous framework walls. Lowering the temperature at the beginning of the reaction increases the exothermicity of the reaction of intermetallic phases synthesis, increases the duration of the peritectic reaction and, as a result, enlarges the zones of peritectic crystallization. Dispersed refractory $NiAl_3$ and $TiAl_3$ compounds synthesized in the course of a heterogeneous reaction have higher crystallization temperatures than TiNi, 1133 °C, and 1340 °C, respectively [14]. This increases the surface tension, reduces the fluidity of the melt and the speed of the synthesis wave propagation, and increases the accumulation of the exothermic reaction heat in the reaction zone.

The proportion of phases with an admixture of aluminum in the peritectic melt increases with aluminum concentration due to the action of a directed crystallization front. The additive action of these

two factors leads to a nonlinear effect of the Al concentration on the geometric and structural homogeneity of the porous alloy, and hence on the stress-strain characteristics.

4. Conclusions

It has been found that alloying porous NiTi SHS alloys with aluminum is promising in terms of improving their deformation and strength properties. The following conclusions can be drawn:

1. The optimal concentration range of doping porous alloys NiTi with Al is 0.5–1 at %. These results are based on the Hume-Rothery dimensional and electronic factors analysis, along with structural studies demonstrating the alloys' strength increase with aluminum addition, which decreases the melting temperature and results in a longer interaction of the reaction components.
2. In porous SHS NiTi alloyed with aluminum, intermetallic TiNi(Al) and Ti_2Ni(Al) phases were observed, and a two-fold increase in the aluminum content in the Ti_2Ni phase was accompanied by an increase in microhardness.
3. An increase in the tensile strength of porous SHS $Ti_{50}Ni_{49}Al_1$ alloy was found, which is due to the TiNi and Ti_2Ni intermetallic phases dispersion strengthening, the formation of the homogeneous finely porous alloy skeleton with a maximum specific surface area, a maximum effective cross-sectional area, and an increased number of bridges with 1–20 μm predominant size.

CRediT authorship contribution statement

Alexander N. Monogenov: Conceptualization, Methodology, Writing – original draft. **Ekaterina S. Marchenko:** Data curation, Supervision, Project administration, Funding acquisition, Methodology. **Gulsharat A. Baigonakova:** Visualization, Investigation, Methodology. **Yuri F. Yasenchuk:** Methodology, Data Curation, Writing – review & editing. **Alex A. Volinsky:** Methodology, Writing – review & editing, Validation, Supervision. **Alexander S. Garin:** Visualization, Investigation.

Data Availability

Data are available from the corresponding author upon reasonable request.

Declaration of Competing Interest

The authors declare that they have no known competing financial interests or personal relationships that could have appeared to influence the work reported in this paper.

Acknowledgements

This research was supported by the Mega grant from the Government of the Russian Federation No. 220 of 9 April 2010 (Agreement No. 075-15-2021-612 of 4 June 2021). Microstructure characterization was carried out at Tomsk Regional Core Shared Research Facilities Center of the National Research Tomsk State University (Grant from the Ministry of Science and Higher Education of the Russian Federation 075-15-2021-693 (13.RFC.21.0012)).

References

[1] Y. Yasenchuk, E. Marchenko, G. Baigonakova, A. Obrosov, J.-H. Kang, Study on tensile, bending, fatigue, and in vivo behavior of porous SHS-TiNi alloy used as a bone substitute, Biomed. Mater. 16 (2) (2021) 021001, https://doi.org/10.1088/1748-605X/aba327
[2] O.V. Kokorev, V.N. Khodorenko, A.A. Radkevich, G.T. Dambaev, V.E. Gunter, Development and differentiation of mesenchymal bone marrow cells in porous permeable titanium nickelide implants in vitro and in vivo, Bull. Exp. Biol. Med. 161 (4) (2016) 587–592, https://doi.org/10.1007/s10517-016-3465-4
[3] H. Chen, Z. Zhang, X.H. Hao, B.X. Huang, X.C. Zhao, C.C. Hu, Microstructure and tribocorrosion properties of NiTi/$AlNi_2Ti$ ternary intermetallic alloy, Vacuum 184 (2021) 109928, https://doi.org/10.1016/j.vacuum.2020.109928
[4] M.J. Garcia-Ramirez, R. Lopez-Sesenes, I. Rosales-Cadena, J.G. Gonzalez-Rodriguez, Corrosion behaviour of Ti-Ni-Al alloys in a simulated human body solution, J. Mater. Res. Technol. 7 (3) (2017) 223–230, https://doi.org/10.1016/j.jmrt.2017.07.003
[5] C. Haixiang, K. Dejun, Comparison on electrochemical corrosion performances of arc and laser thermal sprayed Al-Ti-Ni coatings in marine environment, Mater. Chem. Phys. 251 (2020) 123–200, https://doi.org/10.1016/j.matchemphys.2020.123200
[6] L.J. Meng, Y. Li, X.Q. Zhao, J. Xu, H.B. Xu, The mechanical properties of intermetallic Ni50-xTi50Alx alloys (x j 6,7,8,9), Intermetallics 15 (2007) 814e818.
[7] K.P. Sidnov, D.S. Belov, A.V. Ponomareva, I.A. Abrikosov, A.M. Zharmukhambetova, N.V. Skripnyak, N.V. Mukasyan, Effect of alloying on elastic properties of ternary Ni-Al-Ti system: experimental validation, J. Alloy. Compd. 688 (2016) 534–541, https://doi.org/10.1016/j.jallcom.2016.07.051
[8] K. Edalati, T. Daio, Z. Horita, K. Kishida, H. Inui, Evolution of lattice defects, disordered/ordered phase transformations and mechanical properties in Ni-Al-Tiintermetallics by high-pressure torsion, J. Alloy. Compd. 563 (2013) 221–228, https://doi.org/10.1016/j.jallcom.2013.02.128
[9] Z. Zhou, Z. Zhang, Y. Chen, X. Liang, B. Shen, Composition optimization of Al-Ni-Ti alloys based on glass-forming ability and preparation of amorphous coating with good wear resistance by plasma spray, Surf. Coat. Technol. 408 (2021) 126–800, https://doi.org/10.1016/j.surfcoat.2020.126800
[10] S.-C. Duan, X. Shi, M.-C. Zhang, B. Li, G.-X. Dou, H.-J. Guo, J. Guo, Determination of the thermodynamic properties of Ni-Ti, Ni-Al, and Ti-Al, and nickel-rich Ni-Al-Ti melts based on the atom and molecule coexistence theory, J. Mol. Liq. 294 (2019) 111462, https://doi.org/10.1016/j.molliq.2019.111462
[11] B. Wierzba, Phase competition in ternary Ti-Ni-Al system, Phys. A: Stat. Mech. Appl. 454 (2016) 110–116, https://doi.org/10.1016/j.physa.2016.02.068
[12] N. Travitzky, I. Gotman, N. Claussen, Alumina–Ti aluminide interpenetrating composites: microstructure and mechanical properties, Mater. Lett. 57 (2003) 3422–3426, https://doi.org/10.1016/s0167-577x(03)00090-9
[13] S. Tang, Y. Li, Y. Gao, Q. Zheng, Z. Liu, X. Ren, First-principles investigations of the structural, anisotropic mechanical, thermodynamic and electronic properties of the AlNi2Ti, compound, Crystals 8 (2018) 93, https://doi.org/10.3390/cryst8020093
[14] J.C. Schuster, Z. Pan, S. Liu, F. Weitzer, Y. Du, On the constitution of the ternary system AlNiTi, Intermetallics 15 (2007) 1257e1267.
[15] H. Sina, K.B. Surreddi, S. Iyengar, Phase evolution during the reactive sintering of ternary Al–Ni–Ti powder compacts, J. Alloy. Compd. 661 (2016) 294–305, https://doi.org/10.1016/j.jallcom.2015.11.105
[16] N. Resnina, S. Belyaev, A. Voronkov, A. Gracheva, Mechanical behaviour and functional properties of porous Ti-45 at % Ni alloy produced by self-propagating high-temperature synthesis, Smart, 055-018, Mater. Struct. 25 (5) (2016), https://doi.org/10.1088/0964-1726/25/5/055018
[17] Z. Guo, H. Xie, F. Dai, H. Qiang, L. Rong, P. Chen, F. Huang, Compressive behavior of 64% porosity NiTi alloy: an experimental study, Mater. Sci. Eng.: A 515 (1–2) (2009) 117–130, https://doi.org/10.1016/j.msea.2009.03.083
[18] M. Barrabés, P. Sevilla, J.A. Planell, F. JGil, Mechanical properties of nickel-titanium foams for reconstructive orthopedics, Mater. Sci. Eng.: C. 28 (1) (2008) 23–27, https://doi.org/10.1016/j.msec.2007.02.001
[19] S.L. Zhu, X.J. Yang, F. Hu, S.H. Deng, Z.D. Cui, Processing of porous TiNi shape memory alloy from elemental powders by Ar-sintering, Mater. Lett. 58 (19) (2004) 2369–2373, https://doi.org/10.1016/j.matlet.2004.02.017
[20] H. Aihara, J. Zider, G. Fanton, T. Duerig, Combustion synthesis porous nitinol for biomedical applications, Int. J. Biomater. (2019) 1–11, https://doi.org/10.1155/2019/4307461
[21] R. Rosa, L. Trombi, A. Casagrande, F. Cugini, C. Leonelli, P. Veronesi, On the versatility and distinctiveness in the use of microwave energy for the ignition of low exothermic Ni-Tiintermetallics combustion synthesis, Mater. Chem. Phys. 233 (2019) 220–229, https://doi.org/10.1016/j.matchemphys.2019.05.028
[22] M. Eskil, The effect of aging temperature on transformation parameters of porous NiTi shape memory alloy fabricated by SHS, Russ. J. Non-Ferr. Met. 54 (1) (2013) 104–111, https://doi.org/10.3103/S1067821213010069
[23] V.I. Itin, Shape-Memory Alloys, 2017, 270–271. ⟨https://doi.org/10.1016/B978–0-12–804173-4.00121–6⟩.
[24] Hung-Hua Sheu Le-Chun Hsiung, A comparison of the phase evolution in Ni, Al, and Ti powder mixtures synthesized by SHS and MA processes, 0–325, J. Alloy. Compd. 479 (1–2) (2009), https://doi.org/10.1016/j.jallcom.2008.12.080
[25] G.P. Cammarota, A. Casagrande, G. Poli, P. Veronesi, Ni–Al–Ti coatings obtained by microwave assisted SHS: effect of annealing on microstructural and mechanical properties, Surf. Coat. Technol. 203 (10–11) (2009) 1429–1437, https://doi.org/10.1016/j.surfcoat.2008.11.017
[26] S.C. Duan, X. Shi, M.C. Zhang, B. Li, G.X. Dou, H.J. Guo, J. Guo, Determination of the thermodynamic properties of Ni-Ti, Ni-Al, and Ti-Al, and nickel-rich Ni-Al-Ti melts based on the atom and molecule coexistence theory, J. Mol. Liq. (2019) 111–462, https://doi.org/10.1016/j.molliq.2019.111462
[27] M. Kilic, I. Kirik, M. Okumus, Microstructure examination of functionally graded NiTi/NiAl/Ni3Al intermetallic compound produced by self-propagating high-

temperature synthesis, Met. Mater. 55 (2) (2017) 97–106, https://doi.org/10.4149/km_2017_2_97
[28] Y. Kopit, The ability of systems based on Ni, Al and Ti to be synthesized by self-propagating high-temperature synthesis (SHS), Intermetallics 9 (2001) 387–393, https://doi.org/10.1016/s0966-9795(01)00013-9
[29] M. Sharma, B.C. Maji, M. Krishnan, A study on the phase transformation behavior of Al substituted Ni-rich and Ti-rich Ni–Ti–Al alloys, Phys. Procedia 10 (2010) 28–32, https://doi.org/10.1016/j.phpro.2010.11.070
[30] V. Gunther, Y. Yasenchuk, T. Chekalkin, E. Marchenko, S. Gunther, G. Baigonakova, V. Hodorenko, J. Kang, S. Weiss, A. Obrosov, Formation of pores and amorphous-nanocrystalline phases in porous TiNi alloys made by self-propagating high-temperature synthesis (SHS), S092188311830387X, Adv. Powder Technol. 30 (4) (2019) 673–680, https://doi.org/10.1016/j.apt.2018.12.011
[31] Y. Yasenchuk, V. Gunther, E. Marchenko, T. Chekalkin, G. Baigonakova, V. Hodorenko, S. Gunther, J. Kang, S. Weiss, A. Obrosov, Formation of mineral phases in self-propagating high-temperature synthesis (SHS) of porous TiNi alloy, Mater. Res. Express 6 (5) (2019) 056522, https://doi.org/10.1088/2053-1591/ab01a1
[32] A.Y. Al-Maharma, P.P. Sandeep, M. Bernd, Effects of porosity on the mechanical properties of additively manufactured components: a critical review, Mater. Res. Express 7 (2020) 122001, https://doi.org/10.1088/2053-1591/abcc5d
[33] N.H. Astuti, N.A. Wibowo, M.R.S.S.N. Ayub, The porosity calculation of various types of paper using image analysis, J. Pendidik. Fis. Indones. 14 (1) (2018) 46–51, https://doi.org/10.15294/jpfi.v14i1.9878
[34] L.L. Meisner, Crystal-chemical aspects of the stability of the ordered phase B2 in volume alloying of TiNi, shape memory alloys: properties, technologies, Opportunities 82 (2015) 554–574.
[35] D.R. Lide, CRC Handbook of Chemistry and Physics, 84th edition.,, CRC Press, Boca Raton, Florida, 2003 Section 1, Basic constants, units, and conversion factors; electron configuration of neutral atoms in the ground state. (elements 1–104) 23. W. Hume-Rothery, The structure of metals and alloys, Inst. Metals, London, 1954.
[36] V.E. Gunther, Y.F. Yasenchuk, S.V. Gyunter, E.S. Marchenko, M.M. Iuzhakov, Biocompatibility of porous SHS-TiNi, Mater. Sci. Forum 970 (2019) 320–327.
[37] U. Basheer, D. Vikraman, K. Karuppasamy, Structure, microstructure, and some selected mechanical properties of Ti-Ni Alloys (http://doi), Recent Adv. Metall. Eng. Electrodepos. 10 (5772) (2020) 77535, https://doi.org/10.5772/intechopen.86717
[38] M.S. de Oliveira Araújo, P.C.S. da Silva, C.J. de Araújo, Mechanical behavior and fatigue life of micro welded joints obtained by TIG spots in NiTi wires, Smart Mater. Struct. 28 (12) (2019) 125008, https://doi.org/10.1088/1361-665x/ab4e0f
[39] S.S. Mani Prabu, H.C. Madhu, C. Perugu, K. Akash, K.P. Ajay, Kumar, S.V. Kailas, M. Anbarasu, I.A. Palani, Microstructure, mechanical properties and shape memory behaviour of friction stir welded nitinol, Mater. Sci. Eng. A 693 (2017) 233–236, https://doi.org/10.1016/j.msea.2017.03.101
[40] L. Kahloul, H. Chadli, N. Beliardouh, M. Bououdina, Cold pressing dependence on microstructure and electrochemical performance of porous TiNi alloy, Mater. Res. Express 6 (9) (2019) 096559, https://doi.org/10.1088/2053-1591/ab3023
[41] N. El-Bagoury, Comparative study on microstructure and martensitic transformation of aged Ni-rich NiTi and NiTiCo shape memory alloys, Met. Mater. Int. 22 (3) (2016) 468–473, https://doi.org/10.1007/s12540-016-5603-y
[42] A. Oliveira, M. Kaviany, Role of inter- and intraparticle diffusion in 659 non-uniform particle size gasless compacted-powder combustion synthesis-I: 660 formulation, Int. J. Heat. Mass Transf. 42 (1999) 1059–1073 doi.org/66110.1016/S0017-9310(98)00157-4.
[43] T. Widodo, B. Riyadi, Structure and properties of Ni-Al-Ti systems formed by combustion synthesis, Mater. Sci. Forum 991 (2020) 44–500, https://doi.org/10.4028/www.scientific.net/MSF.991.44
[44] V. Gunther, Yu Yasenchuk, T. Chekalkin, E. Marchenko, S. Gunther, G. Baigonakova, V. Hodorenko, Ji Kang, S. Weiss, A. Obrosov, Formation of pores and amorphous-nanocrystalline phases in porous TiNi alloys made by self-propagating high-temperature synthesis (SHS), Adv. Powder Technol. 30 (2019) 673–680, https://doi.org/10.1016/j.apt.2018.12.011